Effect of Rotational Transform on Thermal Transport in Stellarator-Heliotron Plasmas on LHD

H.Yamada[1,2,*], M.Yokoyama[1,2], R.Seki[1,2], C.Suzuki[1], S.Murakami[3], Y.Yoshimura[1], H.Yamaguchi[1]

[1]*National Institute for Fusion Science, National Institutes of Natural Sciences, Toki, Gifu 509-5292, Japan*

[2]*Department of Fusion Science, SOKENDAI(Graduate University of Advanced Studies), Toki, Gifu 509-5292, Japan*

[3]*Department of Nuclear Engineering, Kyoto University, Kyoto 606-8501*

* Corresponding author: yamada.hiroshi@nifs.ac.jp

Tel. +81-572-58-2342

ORCID iD: 0000-0003-4546-3167

Effect of Rotational Transform on Thermal Transport in Stellarator-Heliotron Plasmas on LHD

Abstract

Experimental evidence that indicates a positive effect of rotational transform on thermal transport has been shown for Electron Cyclotron Heated (ECH) plasmas on Large Helical Device (LHD). Although this positive dependence was suggested by earlier scaling studies on energy confinement time, there was a concern that rotational transform is strongly correlated with another major non-dimensional parameter, that is, aspect ratio, in stellarator-heliotron systems. A careful experiment to exclude correlation between these two non-dimensional parameters was carried out on LHD by means of combining helical coil pitch control and limiter insertion. Plasmas with similar aspect ratio but different rotational transform have been compared in terms of global energy confinement time and local heat diffusivity. Energy confinement time increases with the rotational transform. Also the comparison of plasmas dimensionally similar in terms of normalized gyro-radius, collisionality, normalized pressure and aspect ratio has indicated that thermal transport improves with rotational transform. Since the plasmas studied here are dominated by turbulent transport rather than neoclassical transport, the identified feature, common to toroidal plasmas with tokamak, will stimulate the challenge to resolve the origin of the favorable effect of poloidal field and the compatibility with drift turbulence theory.

Keywords: stellartor-heliotron; rotational transform; aspect ratio; thermal diffusivity; energy confinement time; turbulent transport.

1. Introduction

Magnetic confinement of fusion plasmas in toroidal geometry is essentially based upon the combination of toroidal and poloidal magnetic fields which generate magnetic flux surfaces as well as rotational transform t (= ι/2π = 1/q, where q is the safety factor). While toroidal magnetic fields are generated by external coils for both tokamak and stellarator/heliotron concepts, the difference is that poloidal fields are induced by toroidal plasma current and external twisted coils for tokamak and stellarator/heliotron, respectively.

Neoclassical theory predicts that confinement is improved by increase of t through reduction of the width of banana orbit [1]. Experimentally, energy confinement time certainly increases with the plasma current in tokamak (consequently with t), which is highlighted in the ITER H-mode scaling [1] expression as

$$\tau_E^{IPB98(y,2)} = 0.0562 a^{0.58} R^{1.39} P^{-0.69} \bar{n}^{0.41} B^{0.15} I_p^{0.93} \kappa_a^{0.78},$$

where a, R, P, $\bar{n}_e$, B, I_p and κ_a are minor radius (m), major radius (m), heating power (MW), line averaged density (10^{19}m^{-3}), strength of toroidal magnetic field (T), plasma current (MA) and elongation, respectively. Energy confinement time in stellarator/heliotron also *likely* improves with increase of t [2,3], as can be seen in the expression of the scaling (International Stellarator Scaling 2004, ISS04 in short) [3]:

$$\tau_E^{ISS04} = 0.134 a^{2.28} R^{0.64} P^{-0.61} \bar{n}_e^{0.54} B^{0.84} t_{2/3}^{0.41},$$

where $t_{2/3}$ is the rotational transform at the two-thirds radius. Even if t is taken at different position or averaged, the consequence does not change. Therefore, positive t dependence on energy confinement seems to be robust in nature in toroidal magnetic confinement. However, it should be noted that energy confinement, namely, thermal transport, is dominated by turbulence beyond the neoclassical transport in real plasmas. Although drift turbulence models have been successful in explaining characteristics of thermal transport in a variety of aspects [4], major drift turbulence models predict no or only weak dependence on plasma current, which seems to be inconsistent with experimental observations. While a model of current diffusion ballooning mode has suggested dependence on plasma current [5], corresponding fluctuation has not been identified in experiment yet. No persuasive theoretical explanation other than neoclassical transport is available for stellarator/heliotron, either. Study of dependence of turbulent transport on poloidal fields goes back to the pioneering work by S.Yoshikawa [6], but the origin of the experimentally identified plasma current dependence, in other words, t dependence, still remains unresolved together with isotope effect.

Since stellarator/heliotron generate t by external twisted coils, t and aspect ratio A_p (= R/a) have strong correlation [7,8], which will be discussed in Section 2 in detail. Needless to say, A_p is an important

non-dimensional parameter in the discussion of transport physics. The effect of ι on transport has been studied more specifically in shearless stellarator/heliotron [9]: W7-AS[10], Heliotron-J [11] and TJ-II [12]. When the experiment in shearless stellarator/heliotrons avoids degradation of confinement due to low order rational values of ι resonance, confinement improves at higher ι. However, this dependence can be rephrased by A_p because of strong correlation between these. Therefore, the role of poloidal field in turbulence in stellarator/heliotron has been identified less in experiments to date compared with tokamak, although reports to support a similar trend are available. This article describes a careful experiment to exclude the correlation between two non-dimensional parameters, ι and A_p on LHD [13] and discusses the significance of ι dependence of thermal transport in stellarator/heliotron.

2. Separation of Rotational Transform and Aspect Ratio Dependences

Analytics to average short-wave length variation over the toroidal direction gives the relation $\iota \propto A_p$ [7]. International Stellarator/Heliotron Confinement Database has been compiled from multiple experiments by international collaboration [2,3,14]. Figure 1 shows data distribution of ι and A_p from four machines (CHS [15], LHD, ATF [16] and Heliotron E [17]) in a heliotron/torsatron line which employs a pair of continuous helical windings, which indicates the relation between these two as $\iota_{2/3} \propto A_p^{0.81\pm0.10}$. Table 1 summarizes correlation of major parameters described in the database for these four machines. It can be seen that correlation between ι and A_p is distinguishably high. This means dependence on these two parameters cannot be separated and ι dependence in the scaling expression is statistically unstable. This is the reason for the statement in the Introduction: "Energy confinement time in stellarator/heliotron also *likely* improves with increase of ι." This is in contrast to the clarity in tokamak.

LHD is the world's largest heliotron with major radius of 3.6 m. Major confinement magnetic field is generated by a pair of helical coils with polarity l =2 and toroidal field period M=10. Each helical coil has three current layers which can be controlled independently. Therefore, the effective minor radius can be varied by changing the combination of the coil current in the layers [18]. Here, a pitch parameter of the helical coils is defined by

$$\gamma \equiv \frac{M}{l}\frac{a_c}{R_0}$$

where a_c and R are minor radius and major radius of the current center in the helical coils, respectively. Figure 2 shows ι profiles with different γ. Configuration with smaller γ, which means larger aspect ratio, has larger ι but smaller minor radius. This tendency is natural, as discussed above. Here r_{eff} is the effective minor radius defined by the radius of the circle equal to the area of the corresponding toroidal cross-section of the flux surface. The outermost minor radius is bounded by the separatrix.

Then another tool has been combined with this flexibility of magnetic configuration to break the

constraint between ι and A_p. This is the limiter insertion shown in Fig.3. LHD had a robust horizontally movable head covered by carbon, which was primarily used to study the local island divertor concept [19]. Combined control of the pitch parameter of the helical coils and the position of the limiter head has enabled parameter scan with decoupled ι and A_p. Figure 4 shows the range of variation in the experiment, on the A_p - $\iota_{2/3}$ plane. An open circle and an inverted open triangle are the operational points without limiter insertion for the cases with γ=1.18 and γ=1.25, respectively. Without limiter insertion, there is a clear relation $\iota_{2/3} \propto A_p^{1.48}$.

With limiter insertion, plasma is bounded by the limiter and data shown by closed circles, open and closed triangles have become available. Here minor radius, consequently A_p, is defined by the radius containing 99 % of the total electron kinetic energy which is calculated [20] from electron temperature and density profiles measured by highly spatially resolved Thomson scattering [21]. This minor radius is referred to as a_{99} hereafter. It should be noted that comparison of plasmas with similar A_p but different $\iota_{2/3}$ is possible, as seen in closed circles and closed triangles.

3. Experimental Conditions and Assessment of Rotational Transport Dependence of Energy Confinement Time

Assessment of energy confinement as well as thermal transport under those conditions has been performed for plasmas heated by the centrally focused 2nd harmonic electron cyclotron resonance at the magnetic field of 1.49T and the magnetic axis position R_{ax} of 3.6m. Operational ranges of line averaged density $\overline{n}_e$ and absorbed heating power P are 0.12 - 1.2×$10^{19}$$m^{-3}$ and 0.13 - 0.73MW, respectively. Here, absorbed power is evaluated by the 3D ray tracing code TRAVIS [22]. Since the normalized pressure β is less than 0.2 % even at the maximum, finite β effect on MHD equilibrium and instability can be neglected. Also, radiation loss as well as plasma-limiter interaction are not significant due to low operational density.

Before discussing thermal transport, global energy confinement has been assessed. Since ion temperature profile is unfortunately not available for the present dataset, the stored energy is evaluated by diamagnetic diagnostics [23]. Among parameters in the scaling expression τ_E^{ISS04}, a, R and B are substantially fixed in the present dataset, and dependences on $\overline{n}_e$ and P are robust (see Table 1 confirming sufficient low correlation with other parameters). Therefore, the experimentally evaluated energy

confinement time is normalized by the scaling expression except for $\iota_{2/3}$ dependence so that $\iota_{2/3}$ dependence is extracted.

$$\tau_{E,dia}^{\exp} / \tau_E^{ISS04.w/o.iota} = \tau_{E,dia}^{\exp} / 0.134 a_{99}^{2.28} R^{0.64} P^{-0.61} \bar{n}_e^{0.53} B^{0.84} \ .$$

Figure 5 shows this normalized energy confinement time as a function of $\iota_{2/3}$. Statistical analysis has indicated $\tau_E \propto \iota_{2/3}^{0.70\pm0.13}$. The positive effect ι on global energy confinement has been confirmed independently of the aspect ratio. The power index seems to be stronger than the ISS04 scaling. This is consistent with the local transport analysis discussed in the next section.

4. Comparison of Thermal Transport in Dimensionally Similar Discharges

1-D local heat transport analysis has been performed in order to identify the effect of ι on confinement. In particular, comparison of dimensionally similar plasmas is highlighted. Electron temperature and density profiles are projected to 3-D equilibria [20] and the profile of the heat deposition by ECH is calculated by TRAVIS [22]. Then power balance and heat diffusivity are evaluated by TASK3D-a [24].

Since ion temperature is not available in the present experimental conditions, the ion temperature T_i is assumed to be equal to the electron temperature T_e, and the effective thermal diffusivity χ_{eff} is discussed here. Since the heat is deposited to electrons and the power balance for electrons is primarily investigated, the contribution of equipartition power flow from electrons to ions is a concern. The present procedure can be justified by a power balance analysis using the simulated ion temperature profile. Temperature profiles are simulated by an integrated transport simulation code TASK3D, where the neoclassical transport and the turbulent transport are incorporated [25]. Figure 6 (a) shows the electron and ion temperature profiles from the experiment and the simulation. This is a typical case in which large equipartition power flow is expected among the dataset due to relatively high density (0.9×10^{19}m^{-3}). Simulated electron temperature reproduces experimental observation quite well. Power balance for electrons is compared for the cases with simulated ion temperature and the assumption of $T_i = T_e$ (see Fig.6 (b)). Even for this case with large contribution of equipartition expected, equipartition power flow is not significant and the heat conduction loss is predominant in electron heat transport.

The ISS04 scaling has been derived with constraint of dimensional correctness and its expression can be rewritten in non-dimensional parameters [3] as

$$\tau_E^{ISS04} / \tau_{Bohm} \propto \rho^{*-0.79} \nu^{*0.00} \beta^{-0.19} \iota^{1.06} A_p^{0.07},$$

where τ_{Bhom}, ρ^* and ν^* are the Bohm diffusion time, normalized gyro radius and collisionality normalized

by the bounce frequency of banana trapped particles, respectively. Since energy confinement time and heat diffusivity have a reciprocal relation with each other, the effect of ι on thermal transport can be extracted by comparison of plasmas with the same non-dimensional parameters and different ι. For example, the ISS04 scaling expression suggests $\chi_{eff} / D_{Bohm} \propto \iota^{-1.06}$, where D_{Bohm} is the Bohm diffusivity.

Figure 7 shows two comparisons of dimensionally similar plasmas with different ι for relatively collisional (ν*>1) and collisionless (ν*<1) cases. Results from local thermal transport analysis are shown in Fig.8. Normalized heat diffusivity is larger for low ι than for high ι in both comparisons (see Fig.8(a) and (d)). Figure 8 (b) and (e) show the comparison of experimental results with neoclassical prediction [26]. Since electric field is not considered here, the neoclassical prediction gives the upper limit. It is clear that heat diffusivity in the experiment is significantly larger than the neoclassical prediction for all cases, which means turbulent transport is predominant. Figure 8 (c) and (f) is the power dependence on ι, $\chi_{eff} / D_{Bohm} \propto \iota^{\alpha}$. Even with some excursion, the index α is obviously negative and is located around -1, which clearly indicates the positive effect of ι on thermal transport and supports the expression in the ISS04 scaling.

The global energy confinement is more affected by the local transport in the peripheral region because of the weight in volume integral. The index α clearly falls below 1 in the peripheral region for both comparisons, which suggests stronger dependence on ι than that predicted by ISS04. If the ι dependence of the energy confinement is assumed to $\tau_E \propto \iota_{2/3}^{0.70\pm0.13}$ as seen in Fig.5 with holding other parameter dependences in ISS04, the non-dimensional expression is rephrased into $\tau_E / \tau_{Bohm} \propto \iota^{1.79\pm0.33}$, which leads to $\chi_{eff} / D_{Bohm} \propto \iota^{-1.79\pm0.33}$. This seems to be relevant to the consequence of the local heat transport analysis shown in Fig.8 (c) and (f).

5. Conclusions

The origin of the effect of poloidal fields on turbulent transport has not been understood quite well even for tokamak where clear evidence has been confirmed experimentally. Supportive experimental observations also have been seen in stellarator/heliotron, which is an alternative concept to tokamak and should share common characteristics as toroidal plasmas. However, the rotational transform ι, which is the representing non-dimensional parameter, has strong correlation with the aspect ratio A_p in stellarator/heliotron. Although ι (or q) can be changed via the control of the plasma current without changing A_p in tokamak, such an operation is impossible in general for net-current free plasmas in stellarator/heliotron.

Careful experiment to exclude correlation between these two non-dimensional parameters was carried out on LHD by means of combination of the helical-coil-pitch control and limiter insertion. Low density ECH plasmas are suitable for this study because of centrally focused power deposition and no significant effect of plasma-limiter interaction and radiation loss. It should be noted that turbulent transport surpasses neoclassical transport in these plasmas.

Comparison of plasmas dimensionally similar in terms of normalized gyro-radius, collisionality, normalized pressure and aspect ratio has indicated that thermal transport improves with rotational transform. The survey of plasmas with different ι but the same A_p has indicated that global energy confinement time as well as local heat diffusivity improve with increase of ι independently of A_p. This experimental documentation will contribute to clarification of the origin of the effect of poloidal fields on turbulent transport.

Acknowledgments

The authors are grateful to the LHD Experiment Group and the technical staff of LHD for their support of this work. This work is supported by the National Institute for Fusion Science grant administrative budgets (NIFS14UNTT006, NIFS14KNTT025, NIFS14KLPT004).

References

[1] A.A.Galeev and R.Z.Sagdeev, Sov. Phys. JETP **26**, 233 (1958)
[1] ITER Physics Basis Document, Nucl. Fusion **39**, 2137 (1999)
[2] U.Stroth et al., Nucl.Fusion **36**, 1063 (1996)
[3] H.Yamada et al., Nucl. Fusion **45**, 1684 (2005)
[4] J.W.Connor, H.R.Wilson, Plasma Phys. Control. Fusion **36**, 719 (1994)
[5] K.Itoh, M.Yagi, S-I. Itoh, A.Fukuyama, M.Azumi, Plasma Phys. Control. Fusion **36**, 279 (1993)
[6] S.Yoshikawa, Nucl Fusion **13**, 433 (1973)
[7] M.Wakatani, Stellarator and Heliotron Devices, (Oxford University Press, Inc. 1998), pp.82-100.
[8] K.Nagasaki, K.Itoh, M.Wakatani, A.Iiyoshi, J. Phys. Soc. Jpn. **57**, 2000 (1988)
[9] E.Ascasibar et al., Plasma Fusion Res. **3**, S1004 (2008)
[10] H.Ringler et al., Plasma Phys. Control. Fusion **32**, 933 (1990)
[11] F.Sano et al., Nucl. Fusion **45**, 1557 (2005)
[12] V.I.Vargas et al., Nucl. Fusion **47**,1367 (2007)
[13] A.Komori et al., Fusion Sci. Technol. **58**, 1 (2010)
[14] H.Yamada et al., Fusion Sci. Technol. **45**, 1684 (2005)
[15] K.Nishimura et al., Fusion Technol. **17**, 309 (1990)
[16] J.F.Lyon et al., Fusion Technol. **10**, 179 (1986)

[17] K.Uo et al., Nucl. Fusion **24**, 1551 (1984)
[18] K.Ichiguchi et al., Nucl. Fusion **36**, 1145 (1996)
[19] A.Komori et al., Fusion Eng. Design **39-40**, 241 (1998)
[20] C.Suzuki, et al., Plasma Phys. Control. Fusion **55**, 014016 (2013)
[21] I.Yamada et al., Fusion Sci. Technol. **58**, 345 (2010)
[22] N.Marushchenko et al., Plasma and Fusion Res. **2**, S1129 (2007)
[23] S.Sakakibara, H.Yamada, Fusion Sci. Technol. **58**, 471 (2010)
[24] M.Yokoyama et al., Plasma Fusion Res. **8**, 2403016 (2013)
[25] S.Murakami et al., Plasma Phys. Control. Fusion **57**, 054009 (2015)
[26] C.D.Beidler and W.D.D'haseleer, Plasma Phys. Control. Fusion **37**, 463 (1995)

Figure Captions

Fig.1

Distribution of two variables: rotational transform at two-thirds radius $\iota_{2/3}$ and aspect ratio A_p compiled in the International Stellarator-Heliotron Confinement Database. Contours are density of quantile and the confidence ellipsoid of 95 % is shown by a dashed curve.

Fig.2
Profiles of rotational transform with different pitches of the helical coil in LHD.

Fig.3
Toroidal cross-section at the horizontally elongated position of magnetic flux surfaces and the horizontally movable limiter.

Fig.4

Distribution of two variables: rotational transform at two-thirds radius $\iota_{2/3}$ and aspect ratio A_p for two configurations with different pitches of helical coils with limiter insertion in the present experiment on LHD. An open circle and an inverted open triangle are the cases of vacuum magnetic flux surfaces bounded by separatrix, namely, without limiter insertion. Closed circles and triangles ranging in the same A_p are compared in Fig.5.

Fig.5
Distribution of energy confinement time normalized by the ISS04 scaling without contribution of rotational transform $\iota_{2/3}$ as a function of $\iota_{2/3}$. Symbols correspond to those in Fig.4. Contours are

density of quantile and a dashed line is the statistically fitted line.

Fig.6
(a) Temperature profiles and (b) power balance for electrons in a typical plasma (#81730 at t=1.266s). (a) Solid line, thick dotted line and thin dashed line are T_e in experiment, T_e by simulation and T_i by simulation, respectively. (b) Thick solid line is the deposited heating power by ECH. Dashed lines and dotted lines are loss channels (heat conduction (regular width) and equipartition (thin)) with T_i by simulation and assumption of T_i=T_e, respectively. P_{eq} is obviously zero for the case with T_i=T_e.

Fig.7
Profiles of non-dimensional parameters in two comparisons of dimensionally similar discharges for relatively collisional case (a)-(c) (#81730 at t=1.266s for low ι and #81770 at t=0.666s for high ι) and relatively collisionless case (d)-(f) (#81727 at t=0.666s for low ι and #81771 at t=0.466s for high ι). Rotational transform: ι (a) and (d), collisionality ν*: (b) and (e), and normalized gyro radius ρ*: (c) and (f).

Fig.8
Profiles of effective heat diffusivity normalized by Bohm diffusivity: (a) and (d), comparison of experimental heat diffusivity χ_{eff}^{exp} with neoclassical prediction χ_e^{NC}: (b) and (e), and the index of rotational transform dependence: (c) and (f), in two comparisons of dimensionally similar discharges for relatively collisional case (a)-(c) (#81730 at t=1.266s for low ι and #81770 at t=0.666s for high ι) and relatively collisionless case (d)-(f) (#81727 at t=0.666s for low ι and #81771 at t=0.466s for high ι).

	log P_{abs}	log $\bar{n}_e$	log B	log $\iota_{2/3}$	log A_p
log P_{abs}	1	0.39	-0.14	0.10	-0.14
log $\bar{n}_e$	0.39	1	-0.07	0.07	0.01
log B	-0.14	-0.07	1	0.49	0.46
log $\iota_{2/3}$	0.10	0.07	0.49	1	0.79
log A_p	-0.14	0.01	0.46	0.79	1

Table 1 Correlation coefficient between representative operational parameters in the International Stellarator-Heliotron Confinement Database; absorbed power P, line averaged electron density $\bar{n}_e$,

magnetic field B, rotational transform at two thirds radius $\iota_{2/3}$, and aspect ratio A_p.

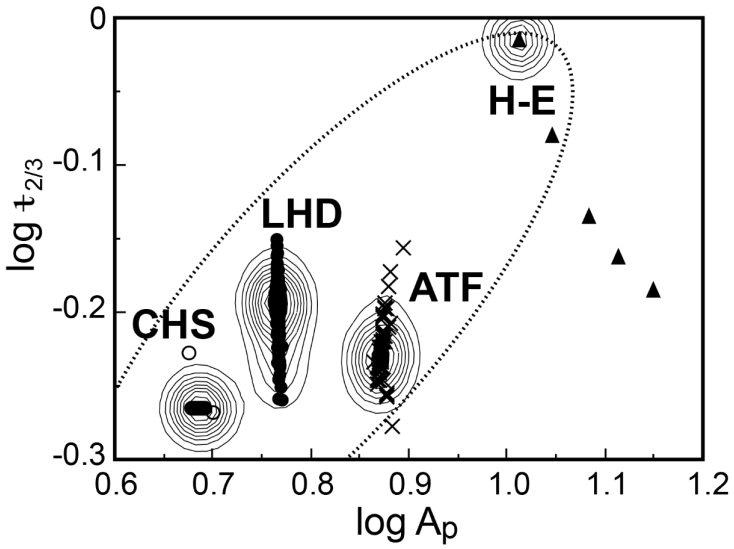

Fig.1

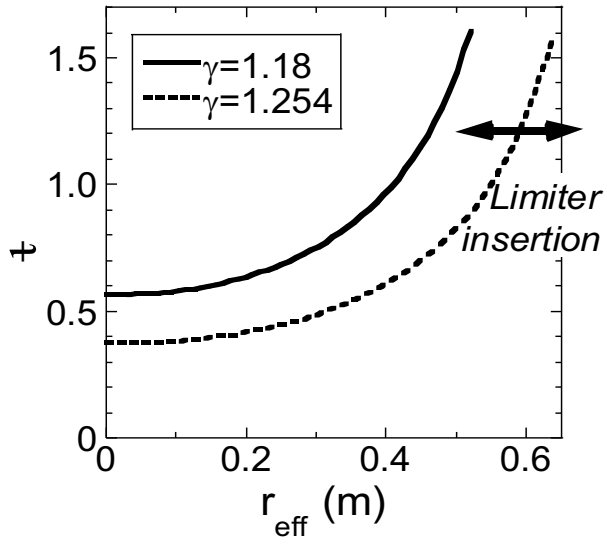

Fig.2

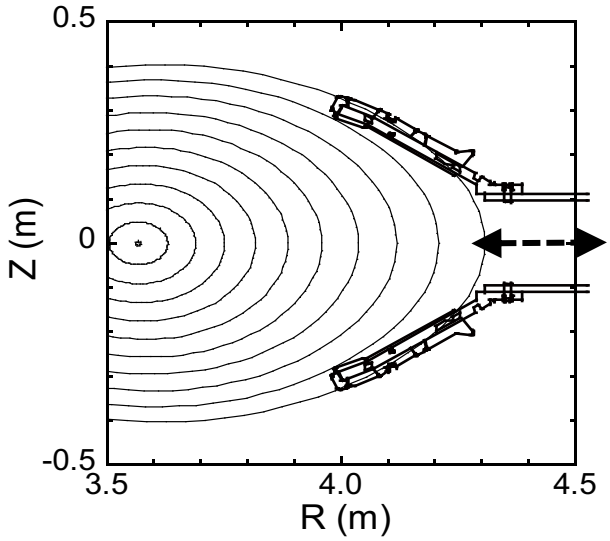
0.5
0
-0.5
Z (m)
3.5
4.0
4.5
R (m)

Fig.3

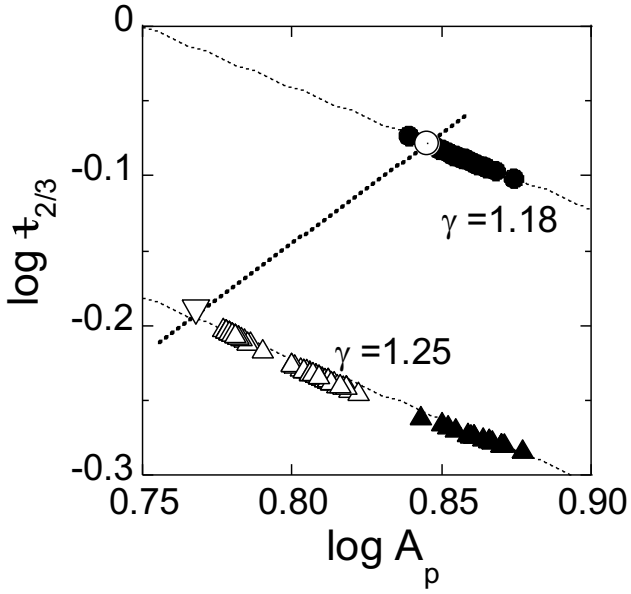
0
-0.1
-0.2
-0.3
log t2/3
γ =1.18
γ =1.25
0.75
0.80
0.85
0.90
log Ap

Fig.4

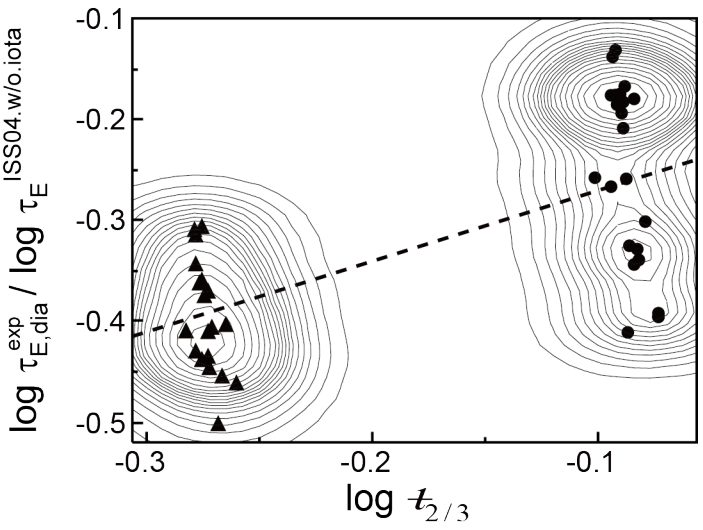
-0.1
-0.2
-0.3
-0.4
-0.5
-0.3
-0.2
-0.1
log $\tau_{E,dia}^{exp}$ / log $\tau_E^{ISS04.w/o.iota}$
log $\iota_{2/3}$

Fig.5

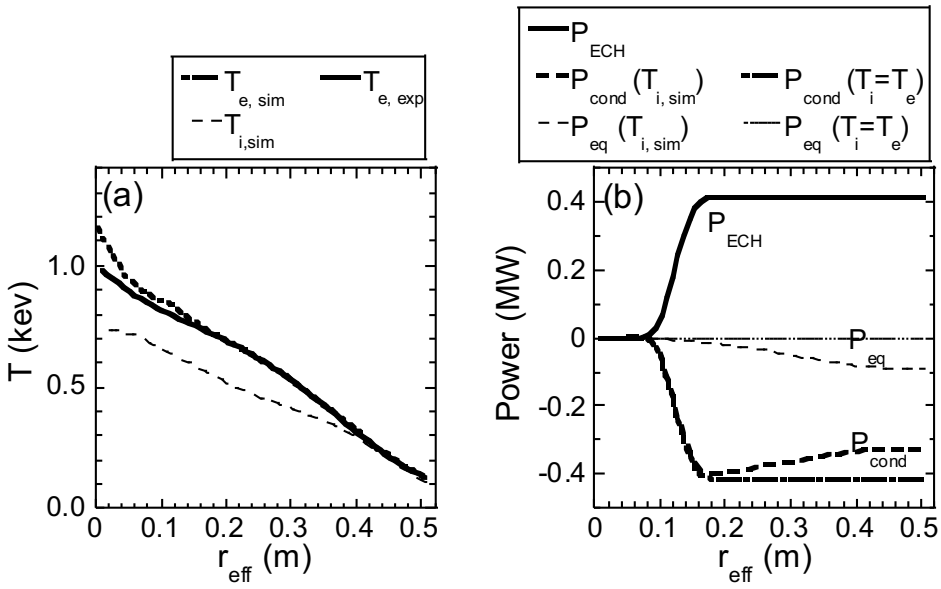
$T_{e,sim}$
$T_{e,exp}$
$T_{i,sim}$
(a)
T (kev)
1.0
0.5
0.0
0
0.1
0.2
0.3
0.4
0.5
r_{eff} (m)
P_{ECH}
$P_{cond}(T_{i,sim})$
$P_{cond}(T_i=T_e)$
$P_{eq}(T_{i,sim})$
$P_{eq}(T_i=T_e)$
(b)
Power (MW)
0.4
0.2
0
-0.2
-0.4
P_{ECH}
P_{eq}
P_{cond}
r_{eff} (m)

Fig.6

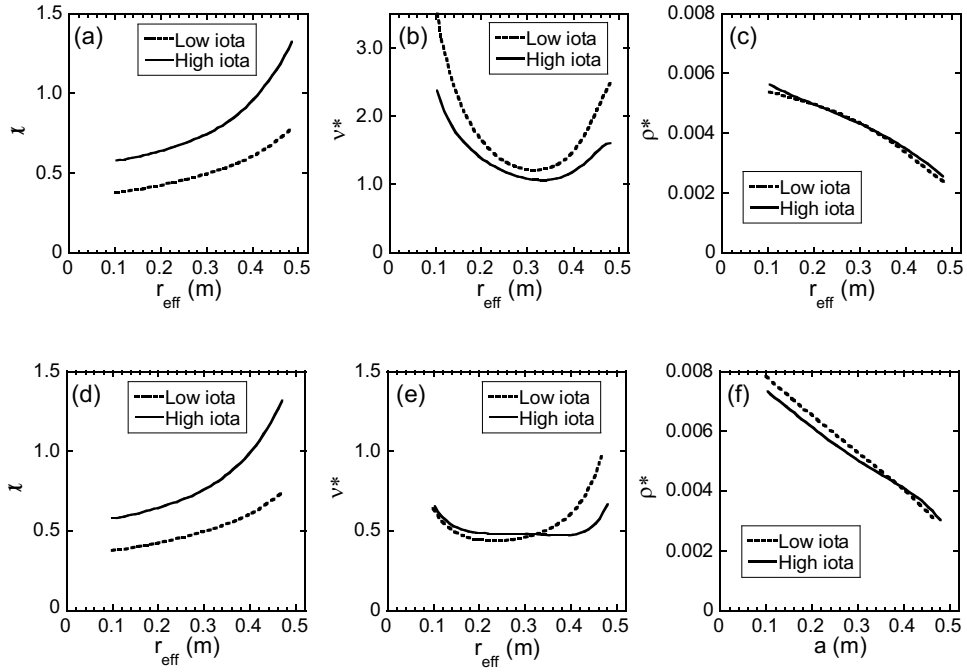
(a)
(b)
(c)
(d)
(e)
(f)
Low iota
High iota
ι
ν*
ρ*
r_eff (m)
a (m)

Fig.7

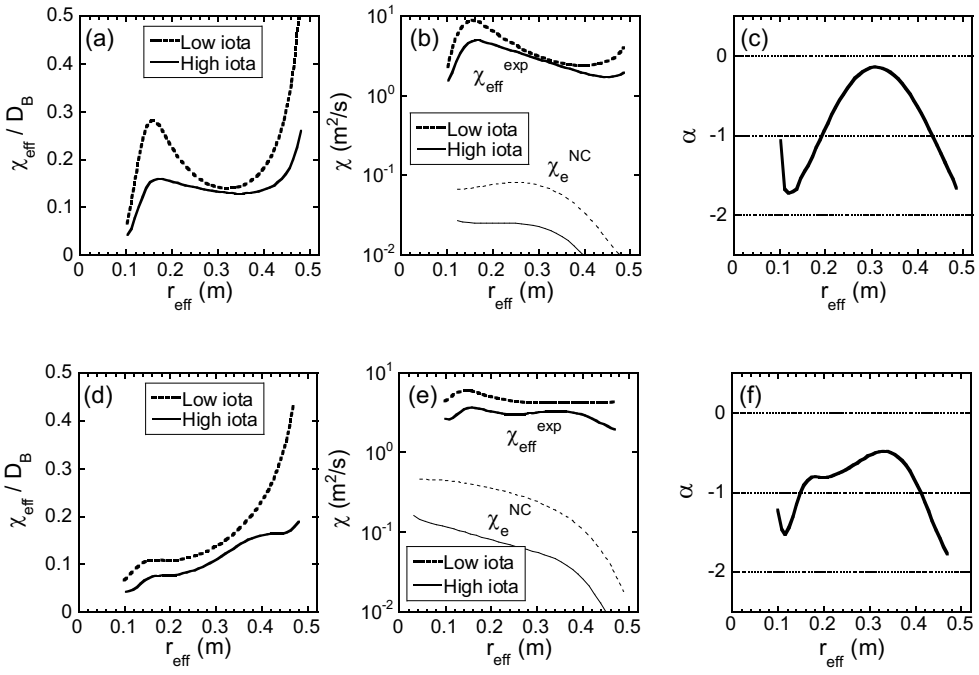
(a)
(b)
(c)
(d)
(e)
(f)
Low iota
High iota
χ_eff / D_B
χ (m²/s)
χ_eff exp
χ_e NC
α
r_eff (m)

Fig.8